厚生労働科学研究費補助金（医療機器開発推進研究事業）
分担研究報告書

「非侵襲的生体膵島イメージングに必要な超高磁場MRIによる膵島撮像法の開発」

研究分担者　松田　哲也　京都大学情報学研究科 教授

研究要旨：　膵島量の定量化を行うための MRI 撮像技術の開発を目的とし、動物用の超高磁場 MRI 装置において単離膵島と他分担研究者によって新規合成された膵島特異的プローブの結合性の評価を行った。GPR40 のリガンドである化合物 GW9508 を用いた検討において、マウスの単離膵島と ^{19}F NMR 信号強度が比例関係にあることを確認した。また GLP-1 受容体のリガンドである化合物 BTFM12 を用いた初期検討でも単離膵島に結合した化合物の ^{19}F MRS 信号検出が可能であった。これらの化合物に対して、結合特異性を検証する実験系での評価を予定している。

A．研究目的

本研究では、糖尿病の超早期診断のために膵島量を定量化する非侵襲的な画像診断法の技術開発を行うことを目的としているが、本分担研究者は動物用の超高磁場 MRI 装置を用いた膵島イメージングを担当し、特に膵島量の定量化に関する MRI 撮像技術の開発を目的としている。

B．研究方法

MRI による膵島量の測定では、小動物用の超高磁場 MRI 装置を用いて、膵島部の位置を識別可能な摘出膵組織切片に対し非造影あるいは Gd 造影剤を用いて膵島描出の検討を行ったが、^{1}H MRI では周囲組織との明瞭な識別が困難であるとの結論を得た。

そこで体内にほとんど存在せず、^{1}H に次いで NMR 検出感度の高い ^{19}F の NMR 信号を利用して MRS/MRI 評価実験を行った。

他分担研究者によって新規合成された ^{19}F を含む分子プローブ溶液にマウスやラットあるいはブタから単離した膵島を暴露し、一定時間後に取り出した膵島を測定サンプルとした。

小動物用 MRI 装置において膵島サンプルの ^{19}F MRS 測定を行い、得られた信号強度と膵島量の関係について調べた。

C．研究結果

GPR40 のリガンドである化合物 GW9508 に対し、暴露するマウスまたはブタの単離膵島量を変え ^{19}F MRS 測定を行ったところ、膵島の数と ^{19}F MRS 信号強度に比例関係があることが確認された。しかし、^{19}F を含まない GPR40 のリガンドを暴露溶液中に添加した化合物 GW9508 の結合特異性の検証実験においては、^{19}F の信号が得られなかった。

また GLP-1 受容体のリガンドである化合物 BTFM12 を用いた検討においても、2×10^{4} 個のマウスの単離膵島に結合した ^{19}F 信号が確認された。化合物 BTFM12 に対し、GLP-1 へのブロッキング実験を行い結合の特異性を検討したが、^{19}F 信号が検出されたり、得られなかったりと一定の結果が得られなかった。

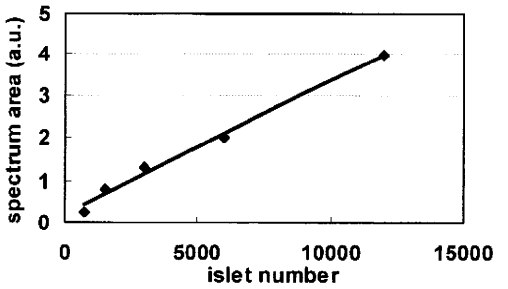

化合物 H の ^{19}F 信号強度と膵島量の関係

D．考察

化合物 GW9508, BTFM12 ともに単離膵島を用いた実験系で信号が確認され、膵島への結合性があることが示唆され、膵島の ^{19}F MR イメージング用プローブとして有用であると考えられる。しかし膵島への特異的な結合については、用いた膵島の種の違いや暴露溶液への溶解性などに問題があり、一定した結果が得られなかった。^{19}F MRI による定量的な評価法としての確立にあたっては、膵島への特異的な結合の確認が必須であり、評価系の確立の必要である。

E．結論

^{19}F MRI による膵島の検出系を提案し、他分担研究者によって合成されたプローブを用いて ^{19}F MRI による膵島イメージングの可能性を示した。定量化に向けたプローブの膵島への特異的結合性の評価の必要性が示唆された。

F．健康危険情報

特になし

G．研究発表

1． 論文発表

1. Takaoka Y, Sakamoto T, Tsukiji S, Narazaki M, Matsuda T, Tochio H, Shirakawa M, Hamachi I, Self-assembling nanoprobes that display off/on ^{19}F nuclear magnetic resonance signals for protein detection and imaging. Nature Chemistry, 1, pp557-561, 2009

2. Tanabe K, Harada H, Narazaki M, Tanaka K, Inafuku K, Komatsu H, Ito T, Yamada H, Chujo Y, Matsuda T, Hiraoka M, Nishimoto S, Monitoring of Biological One-Electron Reduction by ^{19}F NMR Using Hypoxia Selective Activation of an 19F-Labeled Indolequinone Derivative. J Am Chem Soc, 131, pp15982-15983, 2009

2． 学会発表

H．知的財産権の出願・登録状況

1．特許取得

2．実用新案登録

3．その他

厚生労働科学研究費補助金（医療機器開発推進研究事業）
分担研究報告書

「非侵襲的生体膵島イメージングのためのグルコース誘導体の開発」

研究分担者　斉藤美佳子　東京農工大学 共生科学技術研究院 生命機能科学部門

研究要旨：2 型糖尿病患者数は増加の一途をたどっており社会的な問題となっている。糖尿病の超早期診断法の開発には、生体内の膵島量を非侵襲的に計測できるイメージング技術が必要である。本研究では、標的分子として GLUT2 に着目し、その基質である蛍光グルコースに関して高純度、高効率に合成する法について検討を行い重要な知見を得ることができた。本年度は、蛍光グルコースをマウスの各種細胞へ取り込ませその有用性を評価した。

A．研究目的

糖尿病の超早期診断法の開発には、その指標選択が重要なポイントになると考えられる。既に GLUT2 着目した試みもなされているが、超早期の指標として考えるならば、膵島細胞におけるグルコース輸送のダイナミズムを細胞が生きた状態でリアルタイム解析することが必要と考えられる。本研究は、そのような観点から必須のツールである蛍光グルコースの作製と利用法の開発を目的としている。

これまでに、蛍光グルコースの反応材料を Cl-体から F-体に変えることで劇的な改善効果を得ることができ、その化合物の物性、純度、保存条件などについて検討してきた。本年度は、合成された蛍光グルコースを哺乳動物細胞へ適用できるかどうか、その有用性について調べることとした。

B．研究方法

実験に用いた細胞として、マウス ES 細胞と線維芽細胞を用いた。3.5 cm ガラスベースディッシュに播種した細胞を Na HEPES solution で洗浄後、再度 Na HEPES solution を加えて 0~30 分間培養した。Na HEPES solution を除去し、50 μM の 2-NBDG または 2-NBDLG を加え 37℃、5% CO_2、湿度 95% の条件下で培養した。一定時間培養後、2-NBDG または 2-NBDLG を除去し、Na HEPES solution で 2 回洗浄後、培養培地を加え、共焦点顕微鏡により、蛍光画像を取得し ROI ツールで平均蛍光強度を算出し取り込み活性を解析した。さらに、マウス ES 細胞では、未分化状態を維持するために必要な LIF を除いて培養した細胞においても、蛍光グルコースの取り込み活性を解析した。

C．研究結果

マウス ES 細胞および線維芽細胞共に、2-NBDG を細胞内に取り込むことがわかった。2-NBDLG も極わずかながら細胞内に取り込んでいることがわかったが、蛍光強度は、2-NBDG の方が強いことがわかった。また、経時的な解析から ES 細胞と線維芽細胞では 2-NBDG の取り込み方に差が認められ ES 細胞の方が取り込み活性は高かった。さらに、LIF を除いて培養した ES 細胞を用いて 2-NBDG の取り込み活性の変化を測定したところ、分化途中の細胞で最も高い蛍光強度値

を示し、さらに分化が進行すると蛍光強度が減少することが明らかになった。

D．考察

当初、2-NBDLG は細胞膜への吸着と思われる蛍光を回避するためのコントロールとして開発されたものであるが、本実験においては、極わずかなら ES 細胞および線維芽細胞ともに細胞内に取り込んでいることがわかった。共焦点顕微鏡による観察結果から、グルコース輸送体を介した取り込みではなく、エンドサイトーシスによる取り込みではないかと考えられた。2-NBDG の取り込み活性は、ES 細胞の方が線維芽細胞よりもは高かったがこれは、未分化な細胞の方が多くのエネルギーを必要とするためではないかと考えられた。しかし一方、LIF を除いた ES 細胞では、分化途中にある細胞が最も高い蛍光強度値を示したことから、形態の変化など細胞にダイナミックな変化が生じている細胞の方が、代謝を活発化させているために、2-NBDG の取り込み活性が高くなったのではないかと考えられた。

E．結論

蛍光グルコースの取り込み活性を指標に、未分化な細胞と分化した細胞、さらには未分化な細胞と分化過程にある細胞を識別できる可能性があることがわかり、蛍光グルコースが複数の細胞への適用が可能であることがわかりその有用性を示すことができた。

F．健康危険情報

特になし

G．研究発表

1. 論文発表

なし

2. 学会発表

(1)重富知也, 斉藤美佳子, 松岡英明, "生乳中微生物の非培養・培養トレーサブル検出", 日本化学会第８９春季年会, 船橋（2009 年 3 月 29 日）

(2)山本敏弘, 田中伸一, 西内祐二, 豊島 正, 長友克広, 越後瑠夏, 渡邉誠二, 菅 世智子, 水野靖紀, 重富知也, 舟橋久景, 斉藤美佳子, 松岡英明, 山田勝也, "蛍光グルコーストレーサー2-NBDG の対掌体である 2-NBDLG とその誘導体の合成", 第２９回日本糖質学会年会, 高山（2009 年 9 月 11 日）

(3)末崎拓広, 重富知也, 水野靖紀, 島北寛仁, 斉藤美佳子, 舟橋久景, Carl Grenvall, Thomas Laurell, 松岡英明, "Acoustic cell separation technology による食品中微生物のバイアブルセパレーション", 日本防菌防黴学会第３６回年次大会, 大阪（2009 年 9 月 14 日）

(4)重富知也, 末崎拓広, 斉藤美佳子, 舟橋久景, 松岡英明, "食品中微生物の非培養・培養トレーサブル検出", 日本防菌防黴学会第３６回年次大会, 大阪（2009年9月14日）

H．知的財産権の出願・登録状況

1. 特許取得

なし

2. 実用新案登録

なし

3. その他

なし

厚生労働科学研究費補助金（医療機器開発推進研究事業）
分担研究報告書

「非侵襲的生体膵島イメージングによる糖尿病の超早期診断法の開発」

分担研究者　名前　平尾　佳　　所属　アークレイ株式会社　研究開発部第5チーム

研究要旨：　糖尿病の発症過程では、膵島量が耐糖能異常に先行して減少する。この知見に基づき、本研究では糖尿病超早期診断を目的とした、膵島量を測定する非侵襲的画像診断技術の開発を目標とする。このための新規分子プローブの開発を行う。標的分子の探索から開始し、それに基づく分子プローブの設計、作製と実験動物を用いた評価を行う。それに並行して、分子プローブの量産化検討を行う。

A．研究目的

現在、我が国における2型糖尿病は推定740万人を越えて増加し続けており、この対策として耐糖能検査を基準とした糖尿病発症前の介入が行われているが、充分な成果が得られていない。その原因として、機能異常が明らかとなる境界型糖尿病の段階では膵島の障害はすでに高度に進行しており、介入開始時期としては遅い可能性がある。よって、適切な時期の介入を行うための超早期診断の必要性が求められている。

よって、本研究の目的は、糖尿病の超早期診断のために生体内の膵島量を非侵襲的な画像診断法を用いて定量化するための技術開発を行うことである。

B．研究方法

非侵襲的膵島定量に必要な分子プローブの開発と画像診断法の検討を、以下の5つの手順で行う。なお、京都大学分担分については、詳細を割愛した。

1. 膵島イメージング標的分子の選定
2. イメージング分子プローブの設計・開発
3. 標識分子プローブの基礎的評価（*in vitro* ～*ex vivo* まで）
4. *In vivo* における分子プローブの有効性と画像撮像条件の検討

本年度、Exendin-4(9-39)の誘導体4種、Exendin-4の誘導体2種、GW9508の誘導体3種、GW1100の誘導体3種の、計12種類の分子プローブの合成及び標識化を行ない、基礎的評価及び *in vivo* での有効性検討を行なった。

（倫理面への配慮）

動物を用いた実験については、京都大学動物実験に関する指針に基づいて施行する。

C．研究結果

下記12種類の分子プローブ合成・標識化を終了し、有効性検討を行なった。

- GLP-1 受容体アンタゴニスト Exendin-4(9-39)
  : 4種の誘導体の合成・標識化終了。
  基礎評価終了。
- GLP-1受容体アゴニスト Exendin-4
  : 2種の誘導体の合成・標識化終了。
  基礎評価終了。
- GPR40/GPR120 受容体のリガンド GW9508
  : 3種類の誘導体の合成・標識化終了。
  基礎評価終了。
- GPR40受容体のリガンド GW1100

:3種類の誘導体の合成・標識化終了。
基礎評価終了。

D．考察

Exendin-4(9-39)及び Exendin-4 においては、合計 9 種類の誘導体での検討を行なった。

その結果、標識部位、標識時のリンカー等により、分子プローブとしての性能に大きな差が認められた。

しかし、これまでの実験から、性能に影響を与える要因の解明が進んできており、Exendin-4(9-39)及び Exendin-4 の更なる性能向上が可能であると考えられる。

また、GW9508、GW1100 においては、各 3 種類ずつの誘導体で検討を行なったが、脂溶性が高く期待通りの結果を得ることができなかった。

今後、脂溶性を低下させる分子設計が必要であると考える。

E．結論

現状、最も可能性の高い分子プローブは Exendin-4(9-39)及び Exendin-4 誘導体である。

これまでの実験から得られた知見を基に改良を行い、最終的に実用性の高い分子プローブ開発が可能であると確信する。

F．健康危険情報　特になし。

G．研究発表

1.　論文発表

E. Mukai, K. Toyoda, H. Kimura, H. Kawashima, H. Fujimoto, M. Ueda, T. Temma, K. Hirao, K. Nagakawa, H. Saji, and N. Inagaki, GLP-1 receptor antagonist as a potential probe for pancreatic beta-cell imaging. Biochem Biophys Res Commun 389; 523-6, 2009.

2.　学会発表　なし。

H．知的財産権の出願・登録状況

1．特許取得

出願番号：PCT/JP2009/56628
特願2009-68837号
特願2009-68838号
特願2009-68839号
特願2009-204769号
特願2009-228658号
PCT/JP2009/066398
特願2009-185470号

発明の名称：膵島イメージング用分子プローブ前駆体及びその使用（全特許の名称同じ）

2．実用新案登録　なし。

3．その他　なし

Ⅲ. 研究成果の刊行に関する一覧表

書籍

著者氏名	論文タイトル名	書籍全体の編集者名	書　籍　名	出版社名	出版地	出版年	ページ

雑誌

発表者氏名	論文タイトル	発表誌名	巻号	ページ	出版年
E. Mukai, K. Toyoda, H. Kimura, H. et.al.	GLP-1 receptor antagonist as a potential probe for pancreatic beta-cell imaging.	Biochem Biophys Res Commun	389	523-6.	2009
M. Ogura, Y. Nakamura, D. Tanaka, X. et al,	Overexpression of SIRT5 confirms its involvement in deacetylation and activation of carbamoyl phosphate synthetase 1	Biochem Biophys Res Commun	389	Aug. 73	2010
X. Liu, N. Harada, S. Yamane, L. Kitajima, et.al.	Effects of long-term dipeptidyl peptidase-IV inhibition on body composition and glucose tolerance in high fat diet-fed mice.	Life Sci	84	876-81	2010
S.K. Park, L. Amos, A. Rao, M.W. Quasney, et al.	Identification and characterization of a novel ABCA3 mutation.	Physiol Genomics	40	94-9	2010
M. Shimodahira, S. Fujimoto, E. Mukai, et al.	Rapamycin impairs metabolism-secretion coupling in rat pancreatic islets by suppressing carbohydrate metabolism.	J Endocrinol	204	37-46	2010

B. Chapuy, M. Panse, U. Radunski, R. et al.	ABC transporter A3 facilitates lysosomal sequestration of imatinib and modulates susceptibility of chronic myeloid leukemia cell lines to this drug.	Haematologica	94	1528-36.	2009
Noguchi H, Ueda M, Hayashi S, et al.	Comparison of trypsin inhibitors in preservation solution for islet isolation.	Cell Transplant	18(5)	541-7	2009
Sato E, Yano I, Shimomura M, et al.	Larger dosage required for everolimus than sirolimus to maintain same blood concentration in two pancreatic islet transplant patients with tacrolimus.	Drug Metab Pharmacokinet;	24(2)	175-9	2009
Yuasa T, Rivas-Carrillo JD, Navarro-Alvarez N, et al	Neovascularization induced around an artificial device implanted in the abdomen by the use of gelatinized fibroblast growth factor 2.	Cell Transplant	18(5)	683 -8	2009
Kuge Y, Obokata N, Kimura H, et al.	Synthesis and evaluation of a radioiodinated lumiracoxib derivative for the imaging of cyclooxygenase-2 expression.	Nucl Med Biol.	36(8)	869-76	2009
Ono M, Watanabe R, Kawashima H, et al.	Fluoro-pegylated chalcones as positron emission tomography probes for in vivo imaging of beta-amyloid plaques in Alzheimer's disease.	J Med Chem.	52(20)	6394-401	2009
Ono M, Hayashi S, Kimura H, et al.	Push-pull benzothiazole derivatives as probes for detecting beta-amyloid plaques in Alzheimer's brains.	Bioorg Med Chem.	17(19)	7002-07.	2009

Maya Y, Ono M, Watanabe H, et al.	Novel radioiodinated aurones as probes for SPECT imaging of beta-amyloid plaques in the brain.	Bioconjug Chem.	20(1)	95-101	2009
Temma T, Iida H, Hayashi T, et al.	Quantification of regional myocardial oxygen metabolism in normal pigs using positron emission tomography with injectable (15)O-O (2).	Eur J Nucl Med Mol Imaging.	37(2)	377-85	2009
Ogawa K, Kawashima H, Shiba K, et al.	Development of [90Y]DOTA-conjugated bisphosphonate for treatment of painful bone metastases.	Nucl. Med. Biol.	36	129-35	2009
Ogawa K, Kawashima H, Kinuya S, et al.	Preparation and evaluation of 186/188Re- labeled antibody (A7) for radioimmunotherapy with rhenium(I) tricarbonyl core as a chelate site.	Ann. Nucl. Med.	23	843-8	2009
Ueda M, Iida Y, Tominaga A, et al.	Nicotinic acetylcholine receptors expressed in the ventralposterolateral thalamic nucleus play an important role in anti-allodynic effects.	Br J Pharmacol.	159(6)	1201-10	2010
Kudo T, Ueda M, Kuge Y, et al.	Imaging of HIF-1-active tumor hypoxia using a protein effectively delivered to and specifically stabilized in HIF-1-active tumor cells.	J Nucl Med.	50(6)	942-9	2009
Hirokawa Y, Isoda H, Okada T, et al.	Improved Detection of Hepatic Metastases From Pancreatic Cancer Using Periodically Rotated Overlapping Parallel Lines With Enhanced Reconstruction (PROPELLER) Technique After SPIO Administration.	Invest Radiol.	45(3)	158-164,	2010

Nakatani K, Nakamoto Y, Saga T, et al.	The potential clinical value of FDG-PET for recurrent renal cell carcinoma.	Eur J Radiol.		[Epub ahead of print]	2009
Higashi T, Hatano E, Ikai I, et al.	FDG PET as a prognostic predictor in the early post-therapeutic evaluation for unresectable hepatocellular carcinoma.	Eur J Nucl Med Mol Imaging.	37(3)	468-8	2010
Satogami N, Okada T, Koyama T, et al.	Visualization of external carotid artery and its branches: non-contrast-enhanced MR angiography using balanced steady-state free-precession sequence and a time-spatial labeling inversion pulse.	J Magn Reson Imaging	30(3)	678-83	2009
Hara T, Higashi T, Nakamoto Y, et al.	Significance of chronic marked hyperglycemia on FDG-PET: is it really problematic for clinical oncologic imaging?	Ann Nucl Med.	23(7)	657-69	2009
Shimada K, Isoda H, Okada T, et al.	Non-contrast-enhanced hepatic MR angiography: Do two-dimensional parallel imaging and short tau inversion recovery methods shorten acquisition time without image quality deterioration?	Eur J Radiol.		[Epub ahead of print]	2009
Shimada K, Isoda H, Okada T, et al.	Unenhanced MR portography with a half-Fourier fast spin-echo sequence and time-space labeling inversion pulses: preliminary results.	AJR Am J Roentgenol.	193 (1)	106-12	2009

Hirokawa Y, Isoda H, Maetani YS, et al.	Hepatic lesions: improved image quality and detection with the periodically rotated overlapping parallel lines with enhanced reconstruction technique--evaluation of SPIO-enhanced T2-weighted MR images.	Radiology.	251(2)	388-97	2009
Kasahara S, Miki Y, Mori N, et al.	Spin-echo T1-weighted imaging of the brain with interleaved acquisition and presaturation pulse at 3 T: a feasibility study before clinical use.	Acad Radiol.	16(7)	852-7	2009
Gotoh K, Okada T, Miki Y, et al.	Visualization of the lenticulostriate artery with flow-sensitive black-blood acquisition in comparison with time-of-flight MR angiography.	J Magn Reson Imaging.	29 (1)	65-69.	2009
Arizono S, Isoda H, Maetani YS, et al.	High spatial resolution 3D MR cholangiography with high sampling efficiency technique (SPACE): comparison of 3T vs. 1.5T.	Eur J Radiol.	73(1)	114-8	2010
Takaoka Y, Sakamoto T, Tsukiji S, et al.	Self-assembling nanoprobes that display off/on 19F nuclear magnetic resonance signals for protein detection and imaging.	Nature Chemistry,	1,	557-561	2009
Tanabe K, Harada H, Narazaki M, et al.	Monitoring of Biological One-Electron Reduction by 19F NMR Using Hypoxia Selective Activation of an 19F-Labeled Indolequinone Derivative.	J Am Chem Soc,	131	15982-15983	2009

Biochemical and Biophysical Research Communications 389 (2009) 523–526

Contents lists available at ScienceDirect

Biochemical and Biophysical Research Communications

journal homepage: www.elsevier.com/locate/ybbrc

GLP-1 receptor antagonist as a potential probe for pancreatic β-cell imaging

Eri Mukai [a,b], Kentaro Toyoda [a], Hiroyuki Kimura [c], Hidekazu Kawashima [d], Hiroyuki Fujimoto [a,b], Masashi Ueda [e], Takashi Temma [c], Konomu Hirao [f], Kenji Nagakawa [f], Hideo Saji [c], Nobuya Inagaki [a,g,*]

[a] Department of Diabetes and Clinical Nutrition, Graduate School of Medicine, Kyoto University, Kyoto, Japan
[b] Japan Association for the Advancement of Medical Equipment, Tokyo, Japan
[c] Department of Patho-Functional Bioanalysis, Graduate School of Pharmaceutical Sciences, Kyoto University, Kyoto, Japan
[d] Department of Diagnostic Imaging and Nuclear Medicine, Graduate School of Medicine, Kyoto University, Kyoto, Japan
[e] Radioisotopes Research Laboratory, Kyoto University Hospital, Faculty of Medicine, Kyoto University, Kyoto, Japan
[f] Research & Development Division, Arkray, Inc., Kyoto, Japan
[g] CREST of Japan Science and Technology Cooperation (JST), Kyoto, Japan

ARTICLE INFO

Article history:
Received 2 September 2009
Available online 6 September 2009

Keywords:
Glucagon-like peptide-1
Glucagon-like peptide-1 receptor
Exendin-4
Exendin(9-39)
β-Cell imaging
Islet imaging
Molecular imaging
β-Cell mass
Diabetes

ABSTRACT

We examined exendin(9-39), an antagonist of glucagon-like peptide-1 (GLP-1) receptor (GLP-1R), as a potential probe for imaging of pancreatic β-cells. To evaluate *in vitro* receptor specificity, binding assay was performed using dispersed mouse islet cells. Binding assay showed competitive inhibition of [^{125}I]BH-exendin(9-39) binding by non-radioactive exendin(9-39). To assess *in vivo* selectivity, the biodistribution was evaluated by intravenous administration of [^{125}I]BH-exendin(9-39) to mice. Radioactivity of harvested pancreas reached highest levels at 60 and 120 min among organs examined except lung. Pre-administration of excess non-radioactive exendin(9-39) remarkably and specifically blocked the radioactivity of pancreas. After [^{125}I]BH-exendin(9-39) injection into transgenic mice with pancreatic β-cells expressing GFP, fluorescent and radioactive signals of sections of pancreas were evaluated with an image analyzer. Imaging analysis showed that the fluorescent GFP signals and the radioactive signals were correspondingly located. Thus, the GLP-1R antagonist exendin(9-39) may serve as a useful probe for pancreatic β-cell imaging.

Introduction

Type 1 diabetes is an autoimmune disease in which the pancreatic β-cells are almost destroyed, which leads to loss of endogenous insulin secretion. Insulin therapy is therefore required for survival in subjects with type 1 diabetes [1]. Type 2 diabetes is characterized by impaired insulin secretion and insulin resistance, and the pathogenesis is well known to be dependent on a reduction in β-cell function [2]. While a decrease in β-cell mass has been reported in American and Asian type 2 diabetic subjects compared with non-diabetic subjects [3–5], the decrease is small at onset in European subjects, suggesting that the decrease might occur only after onset of the disease [6]. It is therefore unknown whether a decrease in β-cell mass contributes to the development of hyperglycemia that leads to type 2 diabetes. Thus, accurately measuring changes in β-cell mass *in vivo* during diabetes progression is important not only for understanding the pathogenesis but also for facilitating early diagnosis and developing improved treatments for both type 1 and type 2 diabetes.

However, it is difficult to identify islets ranging in size from 50–500 μm in diameter and scattered throughout the pancreas, which is surrounded by abdominal organs. To quantify β-cell mass non-invasively, appropriate probes that can specifically bind to pancreatic β-cells are required. There are previous reports using probes targeting the proteins in β-cells, including sulfonylurea receptor 1 (SUR1) and monoamine transporter 2 (VMAT2) for positron emission tomography (PET) imaging [7]. However, ideal probes for accurate and non-invasive imaging for pancreatic β-cells have not yet been developed.

Glucagon-like peptide 1 (GLP-1) is the incretin peptide released from the intestine in response to nutrient ingestion to augment glucose-induced insulin secretion from pancreatic β-cells through binding to the GLP-1 receptor (GLP-1R) [8,9]. Since GLP-1R is expressed highly in islets, especially on β-cells in pancreas, the ligands of GLP-1R might well be ideal probes for pancreatic β-cell imaging. Because native GLP-1 is degraded rapidly by dipeptidyl peptidase-IV (DPP-IV) distributed throughout the body, DPP-IV-resistant agonistic or antagonistic ligands of GLP-1R [10,11] are preferable to GLP-1 for use as an imaging probe.

In the present study, specific imaging of pancreatic β-cells targeting GLP-1R was evaluated using its antagonist, exendin(9-39), radiolabeled with [^{125}I]-Bolton-Hunter reagent at lysine residues.

* Corresponding author. Address: Department of Diabetes and Clinical Nutrition, Graduate School of Medicine, Kyoto University, 54 Shogoin Kawahara-cho, Sakyo-ku, Kyoto 606-8507, Japan. Fax: +81 75 771 6601.
E-mail address: inagaki@metab.kuhp.kyoto-u.ac.jp (N. Inagaki).

0006-291X/$ - see front matter © 2009 Elsevier Inc. All rights reserved.
doi:10.1016/j.bbrc.2009.09.014

Materials and methods

Radiolabeling of exendin(9-39). [^{125}I]-Bolton-Hunter-labeled exendin(9-39) ([^{125}I]-BH exendin(9-39)) was purchased from Perkin-Elmer (Waltham, MA).

Animals. Six-week-old male ddY mice were obtained from Shimizu Co. (Kyoto, Japan). Transgenic mice expressing green fluorescent protein (GFP) under control of the mouse insulin I gene promoter (MIP) (MIP-GFP mice) were maintained on a C57BL/6 background [12]. Animal care and procedures were approved by the Animal Care Committee of Kyoto University.

Binding assay. The displacing effect of exendin(9-39) on GLP-1R binding was assessed using dispersed islet cells as described previously [13]. Pancreatic islets were isolated from male ddY mice by a collagenase digestion technique [14]. Isolated islets were dispersed using 0.05% trypsin/0.53 mM EDTA (Invitrogen, Carlsbad, CA) and PBS. Islet cells were incubated with [^{125}I]BH-exendin(9-39) (0.1 μCi) in 1 ml of buffer containing 20 mM Hepes (pH 7.4), 1 mM $MgCl_2$, 1 mg/ml bacitracin, and 1 mg/ml BSA for 1 h at room temperature in the presence of varying concentrations of non-radioactive exendin(9-39). Binding was terminated by rapid filtration through Whatman GF/C filters (24 mm) followed by washing three times with 5 ml of ice-cold PBS. The radioactivity of filters was measured in a γ-counter. Results were expressed as the percent radioactivity of bound [^{125}I]BH-exendin(9-39) that remained after addition of non-radioactive compound.

Biodistribution experiments. Biodistribution studies of [^{125}I]BH-exendin(9-39) were performed in male ddY mice. [^{125}I]BH-exendin(9-39) (1 μCi) was administered by tail vein injection. At 15, 30, 60, and 120 min after administration, the mice were sacrificed by exsanguination under anesthesia. Selected organs and blood

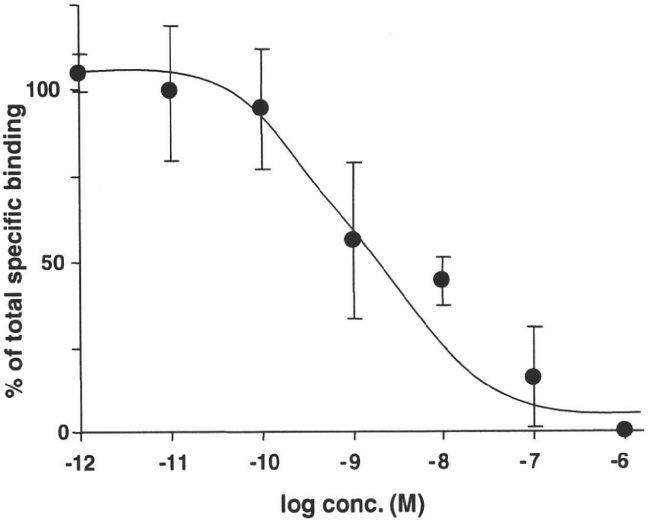

Fig. 1. Binding assay analysis of [^{125}I]BH-exendin(9-39) using mouse pancreatic islet cells. Competitive inhibition of [^{125}I]BH-exendin(9-39) binding by non-radioactive exendin(9-39) is shown. Values are expressed as means ± SD of the percent radioactivity of bound [^{125}I]BH-exendin(9-39) that remained after addition of indicated concentrations of non-radioactive exendin(9-39) (n = 4).

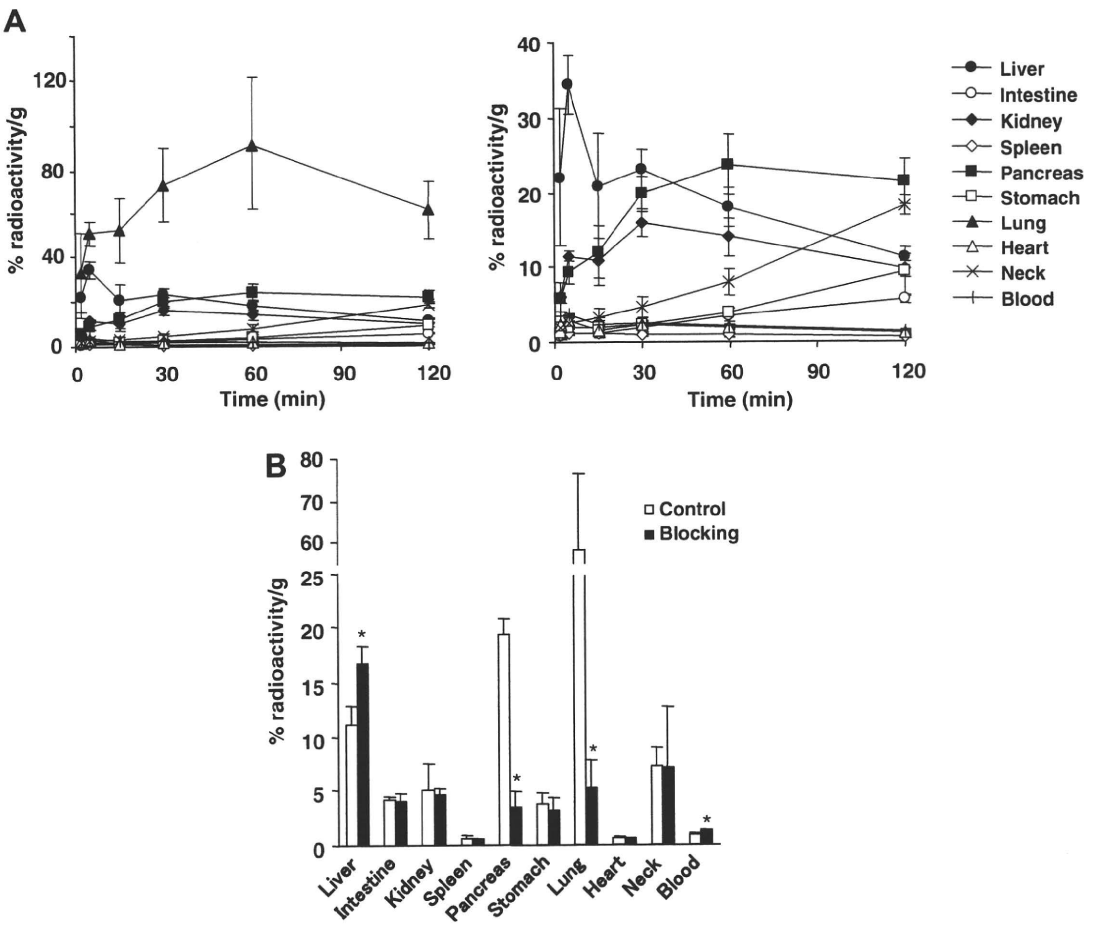

Fig. 2. Tissue distribution of [^{125}I]BH-exendin(9-39) in mice. (A) Time course of tissue distribution of [^{125}I]BH-exendin(9-39). Right graph shows tissue distribution without lung. (B) Blocking of tissue distribution at 120 min after [^{125}I]BH-exendin(9-39) injection by pre-administration of excess non-radioactive exendin(9-39). Values are expressed as means ± SD of the percent radioactivity of injected [^{125}I]BH-exendin(9-39) per gram of organ weight (n = 5). $^{*}P < 0.001$ vs. control.

were harvested and weighed, and the radioactivities were measured with a γ-counter. In a blocking study, excess non-radioactive exendin(9-39) (50 μg) in 100 μl of saline was administered 30 min before the [^{125}I]BH-exendin(9-39) injection. Results were expressed as percent radioactivity of injected [^{125}I]BH-exendin(9-39) per gram of organ weight.

Two-dimensional imaging analysis. After intravenous administration of [^{125}I]BH-exendin(9-39) to male MIP-GFP mice, the pancreas was harvested and cut in several pieces. Each piece was put on slide glass and pressed with a cover glass. Signals of fluorescence and radioactivity (autoradiography) of sections of pancreas were evaluated with an image analyzer (Typhoon 9410; GE Healthcare, Buckinghamshire, UK). The fluorescent and radioactive intensity of each section was analyzed with ImageQuant TL software with resolution of 25 and 10 μm per pixel, respectively (GE Healthcare).

Statistical analysis. Data are expressed as means ± SD. Statistical significance of difference was evaluated by unpaired alternate Welch *t* test. $P < 0.05$ was considered significant.

Results and discussion

We first examined binding specificity of exendin(9-39) to pancreatic β-cell membrane *in vitro*. Binding assay analysis using mouse pancreatic islet cells showed competitive inhibition of [^{125}I]BH-exendin(9-39) binding by non-radioactive exendin(9-39) with a logIC_{50} of −8.84 ± 0.18, similarly to the findings in a previous report [15], indicating that exendin(9-39) binds to those cells specifically (Fig. 1).

To examine selectivity of exendin(9-39) to pancreas *in vivo*, we performed biodistribution studies in mice. Radioactivities of selected organs were measured 15, 30, 60, and 120 min after intravenous administration of [^{125}I]BH-exendin(9-39) (1 μCi). The radioactivity of lung was highest at each time point (Fig. 2A, left panel). Radioactivity of pancreas increased with time and was highest at 60 and 120 min among organs examined excepting lung, and rapid and high binding by liver was observed (Fig. 2A, right panel). To determine whether the binding was specific, we performed blocking study. Pre-administration of excess non-radioactive exendin(9-39) (50 μg) significantly blocked the radioactivities of pancreas and lung to 17.8% and 8.8% of control, respectively, 120 min after [^{125}I]BH-exendin(9-39) injection (Fig. 2B), demonstrating that [^{125}I]BH-exendin(9-39) specifically binds to its receptor in these organs. The binding in other organs such as liver was not blocked by excess non-radioactive exendin(9-39).

To confirm high binding of exendin(9-39) in β-cells, we performed [^{125}I]BH-exendin(9-39) injection in MIP-GFP mice specifically expressing GFP in pancreatic β-cells and imaging analysis of sections of the pancreas removed 60 or 120 min after [^{125}I]BH-exendin(9-39) injection. As shown in Fig. 3A, fluorescent GFP signals were observed in the pancreatic sections of MIP-GFP mice with an image analyzer. Localization of the detected radioactive signals corresponded well to that of the GFP signals, indicating specific high binding of exendin(9-39) in pancreatic β-cells. The intensity of the fluorescent signals of each section also correlated with that of the radioactive signals (Fig. 3B).

Studies for detecting β-cell mass have been performed using probes targeting various β-cell-specific molecules, among which GLP-1R appears promising [7]. *In vivo* imaging of GLP-1R-positive tissues using diethylenetriaminepentaacetic acid (DTPA)-conjugated exendin-4, the GLP-1R agonist, was recently reported [16]. The biodistribution examinations showed its specific binding not only to pancreas and lung but also to stomach. Although pancreas and lung as well as pituitary and adrenals were detected in single photon emission computed tomography (SPECT) imaging, it was not determined whether the probe was confined to β-cells due to the low resolution of the imaging apparatus. In the present study, we found that exendin(9-39), an antagonistic ligand of GLP-1R, has high specificity not only to pancreas but also to β-cells in pancreas, suggesting that β-cell mass can be evaluated. High binding of the probe in lung, as previously reported [16], does not affect analysis of islets because lung is an extra-abdominal organ, for which imaging such as SPECT is required.

A better understanding of the relationship between β-cell mass, β-cell function, and glucose homeostasis by precise measurement of β-cell mass should provide important information on not only for early diagnosis and treatment but also for development of new therapies for intervention strategies. Several tests are presently available for evaluation of β-cell function [17]. In contrast,

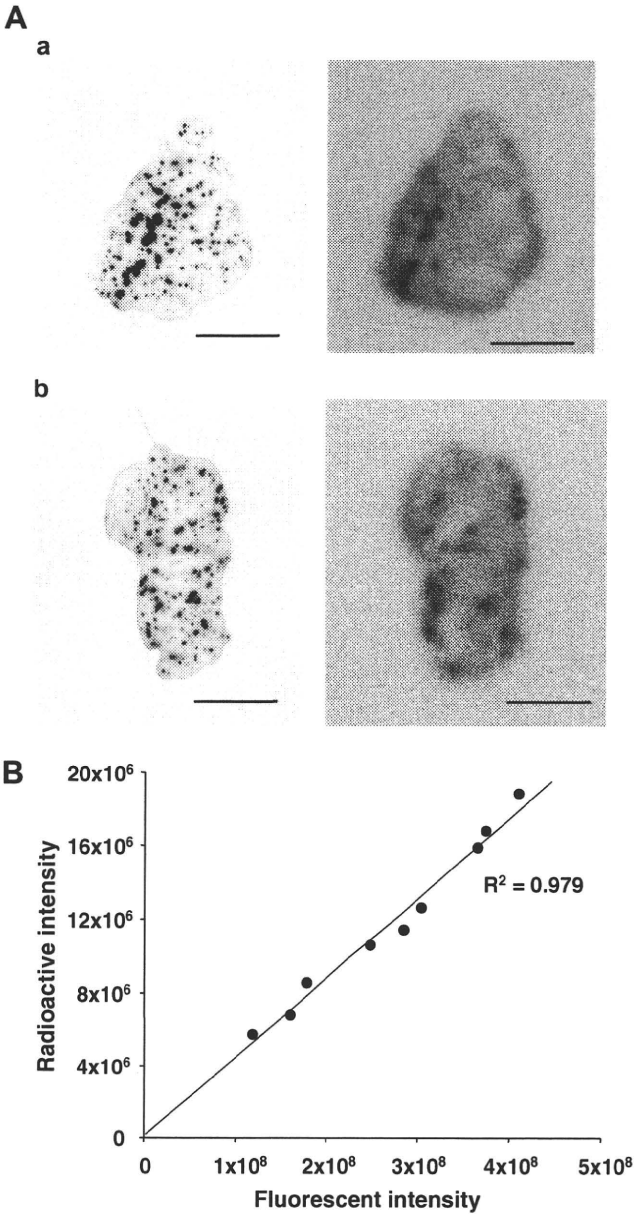

Fig. 3. Imaging analysis of pancreas sections of [^{125}I]BH-exendin(9-39)-injected MIP-GFP mice. (A) Representative fluorescent signals (left panels) and radioactive signals (right panels) of pancreas sections at 60 min (a) and 120 min (b) after [^{125}I]BH-exendin(9-39) injection. Bars represent 1 cm. (B) Correlation of the fluorescent and radioactive intensity. The signal intensity in whole area of each of the nine sections of pancreas harvested 120 min after [^{125}I]BH-exendin(9-39) injection was analyzed with ImageQuant TL software.

measurement of β-cell mass is presently possible only by autopsy. It has recently been reported that antagonistic probes as well as agonistic probes are useful for molecular imaging by targeting peptide receptors [18]. In the present study, we demonstrate for the first time that the GLP-1R antagonist exendin(9-39) is a potential probe for the imaging of pancreatic β-cells.

Acknowledgments

We thank Dr. M. Hara, University of Chicago, for generously providing us transgenic MIP-GFP mice. This work was supported by a Research Grant on Nanotechnical Medicine from the Ministry of Health, Labour, and Welfare of Japan, and by Scientific Research Grants from the Ministry of Education, Culture, Sports, Science, and Technology of Japan, and also by Kyoto University Global COE Program "Center for Frontier Medicine".

References

[1] W.V. Tamborlane, W. Bonfig, E. Boland, Recent advances in treatment of youth with type 1 diabetes: better care through technology, Diabet. Med. 18 (2001) 864–870.
[2] L. Groop, Pathogenesis of type 2 diabetes: the relative contribution of insulin resistance and impaired insulin secretion, Int. J. Clin. Pract. Suppl. (2000) 3–13.
[3] H. Sakuraba, H. Mizukami, N. Yagihashi, R. Wada, C. Hanyu, S. Yagihashi, Reduced beta-cell mass and expression of oxidative stress-related DNA damage in the islet of Japanese type II diabetic patients, Diabetologia 45 (2002) 85–96.
[4] A.E. Butler, J. Janson, S. Bonner-Weir, R. Ritzel, R.A. Rizza, P.C. Butler, Beta-cell deficit and increased beta-cell apoptosis in humans with type 2 diabetes, Diabetes 52 (2003) 102–110.
[5] K.H. Yoon, S.H. Ko, J.H. Cho, J.M. Lee, Y.B. Ahn, K.H. Song, S.J. Yoo, M.I. Kang, B.Y. Cha, K.W. Lee, H.Y. Son, S.K. Kang, H.S. Kim, I.K. Lee, S. Bonner-Weir, Selective beta-cell loss and alpha-cell expansion in patients with type 2 diabetes mellitus in Korea, J. Clin. Endocrinol. Metab. 88 (2003) 2300–2308.
[6] J. Rahier, Y. Guiot, R.M. Goebbels, C. Sempoux, J.C. Henquin, Pancreatic beta-cell mass in European subjects with type 2 diabetes, Diabetes Obes. Metab. 10 (Suppl. 4) (2008) 32–42.
[7] S. Schneider, Efforts to develop methods for in vivo evaluation of the native beta-cell mass, Diabetes Obes. Metab. 10 (Suppl. 4) (2008) 109–118.
[8] L.L. Baggio, D.J. Drucker, Biology of incretins: GLP-1 and GIP, Gastroenterology 132 (2007) 2131–2157.
[9] J.J. Holst, The physiology of glucagon-like peptide 1, Physiol. Rev. 87 (2007) 1409–1439.
[10] J. Eng, W.A. Kleinman, L. Singh, G. Singh, J.P. Raufman, Isolation and characterization of exendin-4, an exendin-3 analogue, from *Heloderma suspectum* venom. Further evidence for an exendin receptor on dispersed acini from guinea pig pancreas, J. Biol. Chem. 267 (1992) 7402–7405.
[11] R. Goke, H.C. Fehmann, T. Linn, H. Schmidt, M. Krause, J. Eng, B. Goke, Exendin-4 is a high potency agonist and truncated exendin-(9-39)-amide an antagonist at the glucagon-like peptide 1-(7-36)-amide receptor of insulin-secreting beta-cells, J. Biol. Chem. 268 (1993) 19650–19655.
[12] M. Hara, X. Wang, T. Kawamura, V.P. Bindokas, R.F. Dizon, S.Y. Alcoser, M.A. Magnuson, G.I. Bell, Transgenic mice with green fluorescent protein-labeled pancreatic beta-cells, Am. J. Physiol. Endocrinol. Metab. 284 (2003) E177–E183.
[13] E. Mukai, H. Ishida, S. Kato, Y. Tsuura, S. Fujimoto, A. Ishida-Takahashi, M. Horie, K. Tsuda, Y. Seino, Metabolic inhibition impairs ATP-sensitive K+ channel block by sulfonylurea in pancreatic beta-cells, Am. J. Physiol. 274 (1998) E38–E44.
[14] R. Sutton, M. Peters, P. McShane, D.W. Gray, P.J. Morris, Isolation of rat pancreatic islets by ductal injection of collagenase, Transplantation 42 (1986) 689–691.
[15] S. Al-Sabah, D. Donnelly, A model for receptor-peptide binding at the glucagon-like peptide-1 (GLP-1) receptor through the analysis of truncated ligands and receptors, Br. J. Pharmacol. 140 (2003) 339–346.
[16] M. Gotthardt, G. Lalyko, J. van Eerd-Vismale, B. Keil, T. Schurrat, M. Hower, P. Laverman, T.M. Behr, O.C. Boerman, B. Goke, M. Behe, A new technique for in vivo imaging of specific GLP-1 binding sites: first results in small rodents, Regul. Pept. 137 (2006) 162–167.
[17] S.E. Kahn, D.B. Carr, M.V. Faulenbach, K.M. Utzschneider, An examination of beta-cell function measures and their potential use for estimating beta-cell mass, Diabetes Obes. Metab. 10 (Suppl. 4) (2008) 63–76.
[18] M. Schottelius, H.J. Wester, Molecular imaging targeting peptide receptors, Methods 48 (2009) 161–177.

Biochemical and Biophysical Research Communications 393 (2010) 73–78

Contents lists available at ScienceDirect

Biochemical and Biophysical Research Communications

journal homepage: www.elsevier.com/locate/ybbrc

Overexpression of SIRT5 confirms its involvement in deacetylation and activation of carbamoyl phosphate synthetase 1

Masahito Ogura, Yasuhiko Nakamura, Daisuke Tanaka, Xiaotong Zhuang, Yoshihito Fujita, Akio Obara, Akihiro Hamasaki, Masaya Hosokawa, Nobuya Inagaki *

Department of Diabetes and Clinical Nutrition, Graduate School of Medicine, Kyoto University, 54 Kawahara-cho, Shogoin, Sakyo-ku, Kyoto 606–8507, Japan

ARTICLE INFO

Article history:
Received 18 January 2010
Available online 25 January 2010

Keywords:
SIRT5
Mitochondria
Urea cycle
Liver

ABSTRACT

SIR2 protein, an NAD-dependent deacetylase, is localized to nucleus and is involved in life span extension by calorie restriction in yeast. In mammals, among the seven SIR2 homologues (SIRT1-7), SIRT3, 4, and 5 are localized to mitochondria. As SIRT5 mRNA levels in liver are increased by fasting, the physiological role of SIRT5 was investigated in liver of SIRT5-overexpressing transgenic (SIRT5 Tg) mice. We identified carbamoyl phosphate synthetase 1 (CPS1), a key enzyme of the urea cycle that catalyzes condensation of ammonia with bicarbonate to form carbamoyl phosphate, as a target of SIRT5 by two-dimensional electrophoresis comparing mitochondrial proteins in livers of SIRT5 Tg and wild-type mice. CPS1 protein was more deacetylated and activated in liver of SIRT5 Tg mice than in wild-type. In addition, urea production was upregulated in hepatocytes of SIRT5 Tg mice. These results agree with those of a previous study using SIRT5 knockout (KO) mice. Because ammonia generated during fasting is toxic, SIRT5 protein might play a protective role by converting ammonia to non-toxic urea through deacetylation and activation of CPS1.

Introduction

SIR2 protein is an NAD-dependent deacetylase [1]. In yeast, increasing the dosage of the SIR2 gene extends life span, whereas disruption of the SIR2 gene shortens it [2]. SIR2 determines life span not only in yeast but also in *Caenorhabditis elegans* [3] and *Drosophila melanogaster* [4]. Mammals have seven SIR2 homologues, SIRT1-7 [5]. SIRT1 deacetylates and regulates the activities of many proteins in the nucleus. SIRT1 upregulates expression of gluconeogenic genes and downregulates glycolytic genes through deacetylation of PPARγ coactivator-1α and FOXO1 [6,7].

SIRT3, SIRT4, and SIRT5 proteins are known to be localized to mitochondria [8]. *In vitro*, SIRT3 protein deacetylates and activates mitochondrial enzymes such as glutamate dehydrogenase, isocitrate dehydrogenase 2, and acetyl CoA synthetase 2 (AceCS2) [9–11]. While SIRT4 does not have NAD-dependent deacetylase activity, it does have ADP-ribosyl transferase activity. SIRT4 inhibits insulin secretion by repression of glutamate dehydrogenase activity through ADP-ribosylation [12,13]. SIRT5 protein also exhibits NAD-dependent deacetylase activity on histone H4 peptide *in vitro* [13]. Recently, Nakagawa et al. reported that SIRT5 interacts with carbamoyl phosphate synthetase 1 (CPS1), and that deacetylated CPS1 is decreased and CPS1 activity is downregulated in livers of SIRT5 knockout (KO) mice [14].

During fasting or starvation, circulating amino acids are derived mainly from catabolism of skeletal muscle, and are used in gluconeogenesis in liver to maintain blood glucose levels. The ammonia co-generated in liver from these amino acids is toxic; the urea cycle detoxifies this ammonia by converting it to non-toxic, water-soluble urea, which is readily excreted from kidney [15,16].

CPS1 is the mitochondrial protein that catalyzes the first step of the urea cycle, the condensation of ammonia with bicarbonate to form carbamoyl phosphate [15,16]. Patients with CPS1 deficiency exhibit lethally severe hyperammonemia in the neonatal period [16], which suggests a critical role for CPS1 in the urea cycle.

In the present study, to investigate the physiological role of SIRT5, we generated SIRT5-overexpressing transgenic (SIRT5 Tg) mice and attempted to identify the target protein of SIRT5 regulation in liver. We show here that SIRT5 protein might regulate urea production by deacetylation and activation of mitochondrial CPS1, complementing the previous study of SIRT5 KO mice [14].

Materials and methods

Animal Experiments: The mice were housed in an air-controlled (temperature 25 °C) room with dark–light cycle (10 h; 14 h).

Abbreviations: SIR2, silent information regulator 2; CPS1, carbamoyl phosphate synthetase 1; Tg, transgenic; KO, knockout.

* Corresponding author. Fax: +81 75 771 6601.
E-mail address: inagaki@metab.kuhp.kyoto-u.ac.jp (N. Inagaki).

0006-291X/$ - see front matter © 2010 Elsevier Inc. All rights reserved.
doi:10.1016/j.bbrc.2010.01.081

Animal care and procedures were approved by the Animal Care Committee of Kyoto University.

Isolation of total RNA and quantitative RT-PCR: Total RNA was isolated from livers, kidneys and hearts of 11 week-old C57BL/6 mice using Trizol (Invitrogen), and cDNA was prepared by reverse transcriptase (Superscript II; Invitrogen) with an oligo (dT) primer. SIRT5 mRNA levels were measured by real-time quantitative RT-PCR using ABI PRISM 7000 Sequence Detection System (Applied Biosystems). SIRT5 mRNA levels were corrected for β-actin mRNA levels. The mouse sequences of forward and reverse primers to evaluate SIRT5 expression were 5′-GTCATCACCCAGAACATCGA-3′ and 5′-ACGTGAGGTCGCAGCAAGCC-3′; respectively. The mouse sequences of forward and reverse primers to evaluate β-actin expression were 5′-TTGCAGCTCCTTCGTTGC-3′ and 5′-CACGAT GGAGGGGAATACAG-3′, respectively. SYBR Green PCR Master Mix (Applied Biosystems) was prepared for PCR run. The thermal cycling conditions were denaturation at 95 °C for 10 min followed by 50 cycles at 95 °C for 15 s and 60 °C for 1 min.

Plasmid construction: The expression vectors for SIRT5 protein with (pCMV5aSIRT5-FLAG) and without (pCMV5aSIRT5) FLAG tag at the C-terminus were constructed as follows. The coding region of mouse SIRT5 cDNA was cloned by PCR using mouse liver cDNA prepared as described above. The PCR fragments were subcloned into pFLAG-CMV-5a (Sigma).

Antibody: SIRT5 polyclonal antibody was produced by immunizing a rabbit with synthetic peptide CGKTLPEALAPHETE, corresponding to 15 C-terminal amino acid residues of mouse SIRT5 protein. The antibody was purified by HiTrap NHS-activated HP kit (GE Healthcare) and gel filtration column. Western blotting analysis was performed using the obtained anti-SIRT5 or anti-FLAG (Sigma) antibodies.

Generation of SIRT5-overexpressing transgenic mice: SIRT5 cDNA with FLAG tag sequences was inserted to the *Eco*RI site of transgenic plasmid pIns-1 [17], and the human insulin promoter of pIns-1 was then replaced by the CAG promoter derived from pCAGGS plasmid [18]. The transgene cassettes were excised from the resulting plasmid by digestion with *Not*I and *Xho*I, and the linearized cassettes were microinjected to fertilized eggs of C57BL/6 inbred mice (PhoenixBio CO., Ltd. Hiroshima, Japan). Since the two lines revealed similar data, all additional experiments were performed using line #38.

Preparation of mitochondria: The livers of C57BL/6 mice were homogenized in isotonic buffer (PBS containing 0.25 M sucrose) containing protease inhibitors (Complete, EDTA free: Roche) with potter homogenizer. The mitochondria were prepared as described previously [8].

Two-dimensional electrophoresis and identification of protein: Liver mitochondria were prepared as described previously [8] and lysed with rehydration buffer (8 M urea, 2% CHAPS, 50 mM DTT, 0.2% Bio-Lyte (BIO-RAD), 0.001% bromophenol blue), and applied to ReadyStrip IPG Strip (BIO-RAD) and separated by isoelectric focusing electrophoresis with a range pH 5 to pH 8 using PROTEAN IEF cell (BIO-RAD). The IPG Strip was then subjected to SDS–polyacrylamide gel electrophoresis. The obtained gel was stained with SYPRO Ruby protein gel stain kit (invitrogen), and the protein was visualized and analyzed using Typhoon 9210 (GE healthcare). The protein at the indicated spot was isolated and analyzed using MALDI-TOF-MS (APRO Life Science Institute, Inc.).

Immunoprecipitation: Mitochondria lysed with PBS containing 1% Triton X-100 were incubated with anti-CPS1 (Santa Cruz) or anti-acetylated lysine (Cell Signaling) antibody for 16 h at 4 °C. Protein G Sepharose (GE healthcare) was then added and incubation was continued for 3 h. The resin was washed and boiled with SDS sample buffer (0.2 M Tris, 10% sucrose, 10% SDS, 5 mM EDTA). The sample was analyzed by western blotting with anti-CPS1 antibody.

Determination of CPS1 activity: Livers of 8–12 week-old SIRT5 Tg and wild-type mice fasted for 16 h were homogenized [19] and CPS1 activities were assayed as described by Fahien and Cohen [20]. Briefly, the reaction was started by adding the supernatant obtained above (enzyme source) to the assay mixture containing 2.5 mM phosphoenopyruvate, 0.2 mM NADH, 10 mM NH_4Cl, 100 mM $KHCO_3$, 5 mM ATP, 10 mM $MgSO_4$, 10 mM *N*-acetylglutamate, 10 U/ml pyruvate kinase (SIGMA), 12.5 U/ml of lactate dehydrogenase (SIGMA), and 50 mM glycylglycine (pH 7.6) at room temperature, and the decrease in absorbance at 340 nm was measured. The initial velocity of the reaction was directly proportional CPS1 activity. One unit of CPS1 activity corresponded to oxidation of 1 μmol of NADH/min at room temperature.

Measurement of hepatic urea production: Hepatocytes of 8–12 week-old SIRT5 Tg and wild-type mice fasted for 16 h were isolated as described previously [21]. Obtained hepatocytes (1.5×10^5) were incubated at 37 °C in humidified atmosphere (5% CO_2) in 2 ml Krebs ringer buffer with 25 mM $NaHCO_3$, 10 mM NH_4Cl, and 5 mM ornithin–HCl [22]. Incubation was stopped by placing the cells on ice, followed by centrifugation at 4 °C for 10 min at 600*g*. The supernatant was removed and urea concentration was measured by diacetyl monoxime methods [23,24], the cells were lysed with 0.1% SDS, and the protein concentration was determined (Bio-Rad Protein Assay Kit).

Statistical analysis: Values are expressed as means ± SEM. Statistical analysis was performed unpaired Student's *t*-test. *P* values <0.05 were considered significant.

Results

Upregulation of SIRT5 mRNA levels by fasting

Expression levels of SIRT1 mRNA are known to be increased in liver and heart by fasting [25]. However, it is unclear whether the expression levels of SIRT5 are regulated by nutrient conditions. To evaluate alteration of SIRT5 mRNA expression levels in different nutrient conditions, total RNA was extracted from organs including liver, kidney, and heart in C57BL/6 mice fed *ad libitum*, fasted for 24 h, or refed for 24 h after 24-h fasting, and quantitative RT-PCR was carried out. SIRT5 mRNA levels in liver were increased 2.4-fold by fasting ($N = 4$, $P < 0.01$) and were decreased to fed condition levels by refeeding ($N = 4$, $P < 0.05$), but were unchanged in kidney or heart (Fig. 1), suggesting an important role of SIRT5 in liver.

Generation of SIRT5 Tg mice

To clarify the function of SIRT5 *in vivo*, we generated SIRT5-overexpressing transgenic (SIRT5 Tg) mice in which expression of mouse SIRT5 fused with FLAG tag at the C-terminus was driven by the CAG promoter (Fig. 2A). Southern blot analysis was performed for genotyping (Fig. 2B), and two independent SIRT5 Tg mouse lines were established on the C57BL/6 inbred background (Fig. 2C). One of these, mouse line #36, was generated with a low copy number of transgene; the other, mouse line #38, was generated with a high copy number of transgene. SIRT5 Tg mice showed no gross anatomical or reproductive defects. In addition, no histological abnormality was observed by light microscopic analysis in all of the organs examined. To investigate the expression of SIRT5 protein, an antibody specific for mouse SIRT5 was raised in a rabbit against a synthetic peptide corresponding to 15 C-terminal amino acid residues (CGKTLPEALAPHETE) of mouse SIRT5, which shows no similarity to other members of the SIRT family. To ascertain specificity of the antibody, mitochondrial proteins were prepared from COS7 cells transfected with the expression plasmid encoding mouse SIRT5 protein fused with FLAG tag,

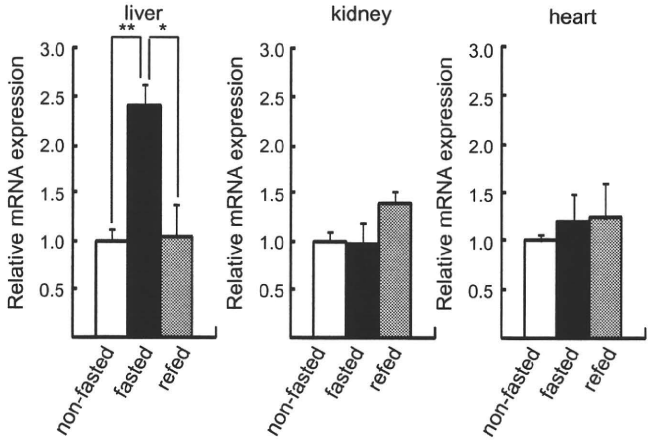

Fig. 1. Alteration of expression levels of SIRT5 mRNA by fasting and refeeding. Total RNA was isolated from livers, kidneys and hearts of 11 week-old C57BL/6 mice. Mice were divided into three groups: non-fasted ($N = 4$, open bars), fasted ($N = 4$, filled bars), and refed ($N = 4$, gray bar). The non-fasted group was fed *ad libitum*, the fasted group was fasted for 24 h, and the refed group was fasted for 24 h followed by normal chow for 24 h. The expression levels of SIRT5 mRNA were estimated by quantitative RT-PCR. SIRT5 mRNA levels were corrected for β-actin mRNA levels. Values are means ± SEM. $^{*}P < 0.05$. $^{**}P < 0.01$.

and western blotting was performed using the obtained anti-SIRT5 antibody or anti-FLAG antibody. A single band at ~32 kDa corresponding to the molecular weight of SIRT5–FLAG protein was detected with each antibody (Fig. 2D), demonstrating that this antibody specifically recognizes SIRT5 protein. Western blot analysis of mitochondrial proteins prepared from livers of the two SIRT5 Tg mouse lines using the anti-SIRT5 antibody showed that both endogenous 32-kDa SIRT5 protein and a SIRT5–FLAG protein with a molecular size somewhat larger were present, and that expression of SIRT5–FLAG protein was more abundant than that of endogenous SIRT5 protein in both Tg mouse lines (Fig. 2E).

Identification of CPS1 as a target of SIRT5 protein

Since SIRT5 mRNA levels were significantly upregulated in liver by fasting, we attempted to identify the protein that is modified by SIRT5 protein in liver. We hypothesized that deacetylation of the SIRT5 target protein might be facilitated by overexpression of SIRT5 in SIRT5 Tg mice. Because NAD-dependent deacetylase converts acetylated lysine to lysine of the target protein, its isoelectric point should shift to a higher pH value. Therefore, we performed two-dimensional electrophoresis to compare mitochondrial proteins prepared from livers of SIRT5 Tg mice and wild-type littermates; the protein samples were applied for isoelectric focusing electrophoresis, and separated by SDS-PAGE followed by staining with SYPRO Ruby. One of the proteins that newly appeared in SIRT5 Tg liver (Fig. 3A, indicated by arrow) was isolated, treated with trypsin, and analyzed by MALDI-TOF-MS (Fig. 3B). The sequences identified by mass spectrometry covered the N-terminal segment of carbamoyl phosphate synthetase 1 (CPS1) (Table. 1), suggesting that the protein is CPS1. CPS1 is a mitochondrial protein

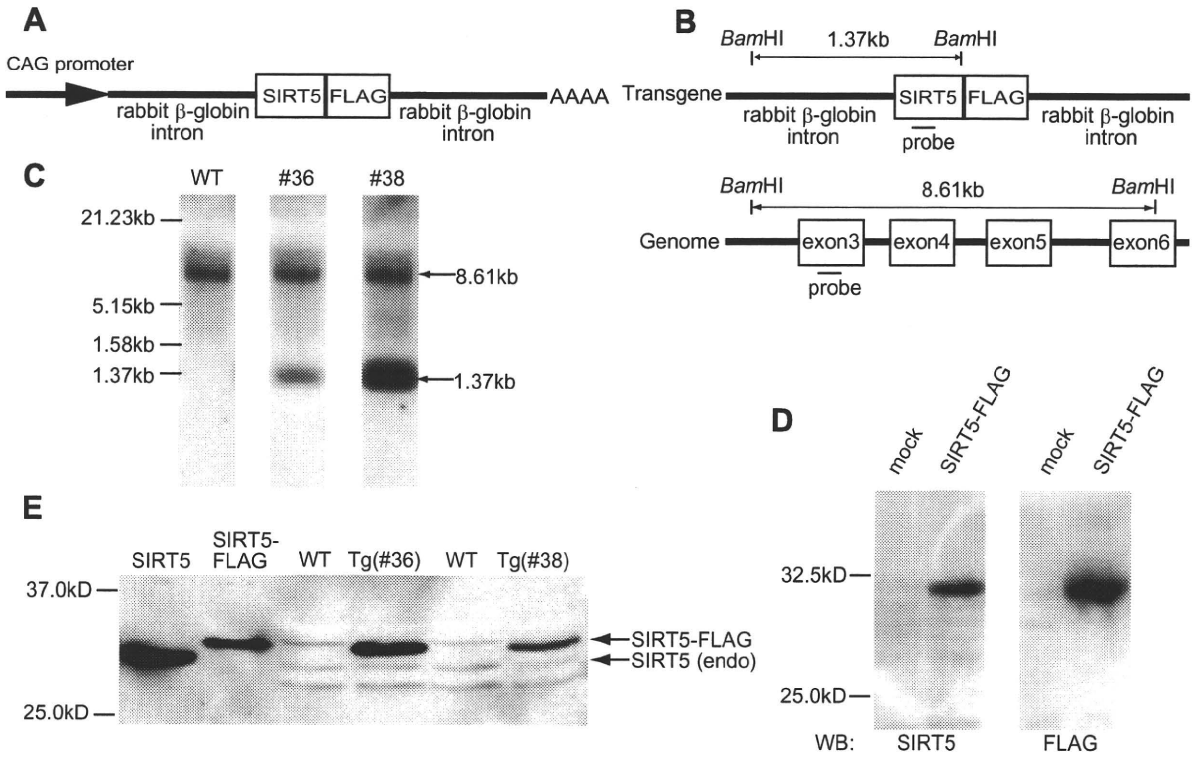

Fig. 2. Generation of SIRT5-overexpressing transgenic (SIRT5 Tg) mice and anti-SIRT5 antibody. (A) Scheme of the transgene used to generate SIRT5 Tg mice. The CAG promoter drives expression of mouse SIRT5 fused with FLAG tag at the C-terminus (SIRT5–FLAG). (B) Location of probes for Southern blot analysis. The probe corresponding to the DNA sequence in exon3 of mouse SIRT5 gene detects an 8.61-kb fragment in genomic DNA and a 1.37-kb fragment in the transgene after digestion with *Bam*HI. (C) Southern blot analysis of *Bam*HI-digested genomic DNA of wild-type (left panel) and SIRT5 Tg mice (middle panel: #36 transgenic mouse line, right panel: #38 transgenic mouse line). Southern blotting was performed with the probe indicated in (B). (D) Ascertainment of anti-SIRT5 antibody. The plasmid encoding mouse SIRT5 protein fused with FLAG tag (pCMV5aSIRT5–FLAG) was transfected to COS7 cells. Mitochondrial proteins were prepared from transfected and mock-transfected cells, and western blotting was performed with anti-SIRT5 antibody (left panel) and anti-FLAG antibody (right panel). (E) Overexpression of SIRT5–FLAG protein in SIRT5 Tg mice. Mitochondrial proteins were prepared from cells transfected with the plasmid encoding mouse SIRT5 without (pCMV5aSIRT5) or with FLAG (pCMV5aSIRT5–FLAG) and from livers of SIRT5 Tg mice and wild-type littermates (#36 and #38 transgenic mouse lines), and western blot analysis was performed using anti-SIRT5 antibody. Endogenous SIRT5 (endo) and SIRT5–FLAG proteins are indicated by arrows.

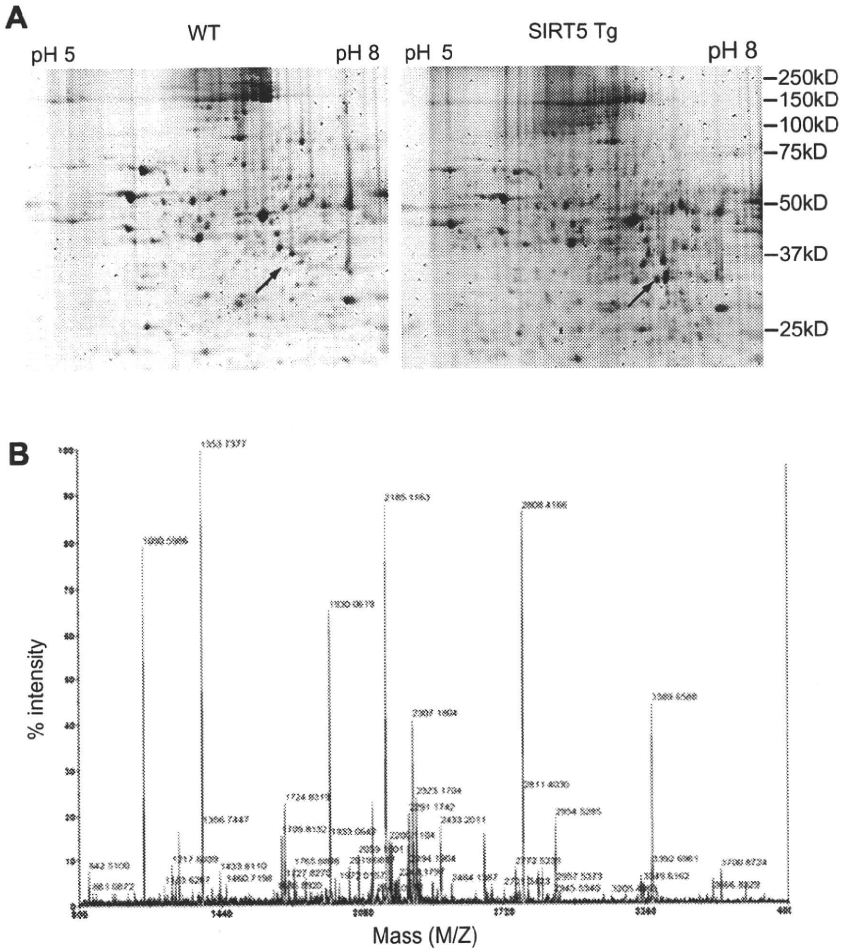

Fig. 3. Identification of the target protein of SIRT5. (A) Two-dimensional electrophoresis of mitochondrial proteins prepared from livers of SIRT5 Tg and wild-type mice. The position of the mitochondrial protein prepared from SIRT5 Tg liver identified by MALDI-TOF-MS is shown by arrow (right panel). The protein is not detected at the corresponding position (indicated by arrow, left panel) in wild-type liver. (B) MALDI-TOF-MS analysis. The mitochondrial protein prepared from SIRT5 Tg liver indicated in (A) was analyzed using MALDI-TOF-MS.

Table 1
Characterization by MALDI-TOF-MS of the target protein of SIRT5.

Measured peptide mass (Da)	Predicted peptide sequence	Start–end
1090.5986	KVPAIYGVDTRM	157–166
1217.6039	KSLGQWLQEEKV	147–156
1353.7377	RGQNQPVLNITNRQ	316–327
1723.8272	KIEFEGQSVDFVDPNKQ	182–196
1930.0619	KEPLFGISTGNIITGLAAGAKS	287–306
2058.1598	RKEPLFGISTGNIITGLAAGAKS	286–306
2184.1154	KGQILTMANPIIGNGGAPDTTARD	90–111
2807.4071	KIEFEGQSVDFVDPNKQNLIAEVSTKD	182–206
2953.5338	KGQILTMANPIIGNGGAPDTTARDELGLNKY	90–118
3662.8010	KMKGYSFGHPSSVAGEVVFNTGLGGYPEALTDPAYKG	55–89

Mass of peptides corresponding to a tryptic digest of CPS1. The corresponding sequence and position (number of amino acid residues) in the sequence are indicated.

expressed predominantly in liver, and catalyzes condensation of ammonia and bicarbonate to carbamoyl phosphate, which is the first step in the urea cycle in liver [15,16].

CPS1 is deacetylated in SIRT5 Tg liver

Since CPS1 is known to be an acetylated protein [26], we investigated deacetylation of CPS1 protein by SIRT5. The mitochondrial protein prepared from livers of SIRT5 Tg and wild-type mice fed *ad libitum* were immunoprecipitated with an anti-acetylated lysine antibody followed by immunoblotting using anti-CPS1 antibody. Acetylated CPS1 protein levels in SIRT5 Tg ($N = 3$) mice were 40% lower than those in wild-type mice ($N = 3$), although total CPS1 expression levels were similar (Fig. 4A). To determine whether SIRT5 protein regulates CPS1 activities, livers of SIRT5 Tg and wild-type mice were homogenized and CPS1 activities were measured. CPS1 activities were significantly increased approximately 2-fold in SIRT5 Tg mice ($N = 5$, $P < 0.01$) compared to those in wild-type mice (Fig. 4B). These results demonstrate that SIRT5 protein deacetylates CPS1 and upregulates its activity in liver.

Urea production is upregulated in SIRT5 Tg hepatocytes

To verify that SIRT5 is involved in the urea cycle by regulating CPS1 activity, production of urea in primary cultured hepatocytes was evaluated. Primary hepatocytes were isolated from SIRT5 Tg and wild-type mice and incubated with ammonia, bicarbonate, and ornithine for 1 h, and the amount of urea synthesized was determined by measuring the urea concentration in the media. Hepatocytes from SIRT5 Tg mice produced more urea than those of wild-type mice (44%, $N = 4$, $P < 0.01$) (Fig. 4C), indicating that urea synthesis is upregulated by overexpression of SIRT5 in liver.

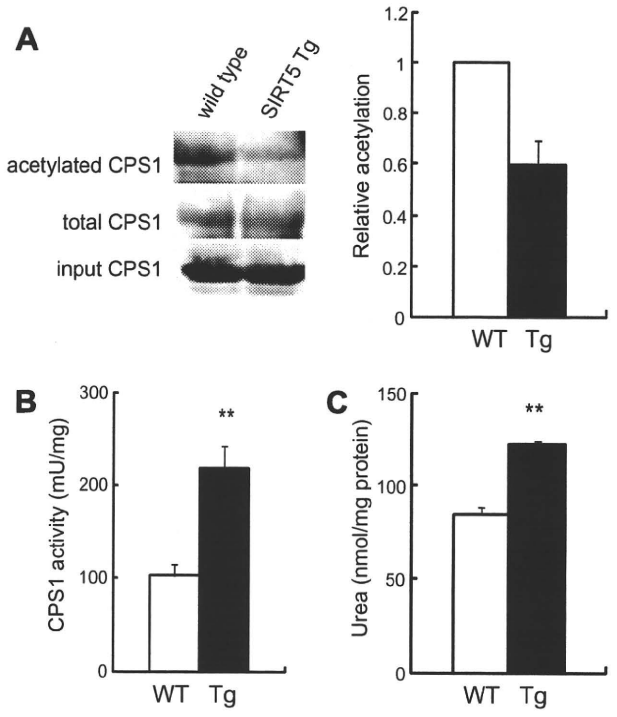

Fig. 4. Deacetylation and activation of CPS1 in livers of SIRT5 Tg mice. (A) CPS1 deacetylation in livers of SIRT5 Tg mice. The mitochondrial protein from livers of SIRT5 Tg and wild-type mice fed *ad libitum* were immunoprecipitated with anti-acetylated lysine antibody (left upper panel) and anti-CPS1 antibody (left middle panel), and immunoblotted with anti-CPS1 antibody. The right panel shows acetylation of CPS1 protein. The ratio of acetylated CPS1 protein of SIRT5 Tg liver to that of wild-type liver was calculated from densitometry of western blots ($N = 3$). (B) Activation of CPS1 activity in SIRT5 Tg liver. Livers of SIRT5 Tg ($N = 5$) and wild-type ($N = 5$) mice fasted for 16 h were homogenized and CPS1 activities were determined as described in Materials and methods. (C) Production of urea in primary cultured hepatocytes. Primary hepatocytes were isolated from SIRT5 Tg ($N = 4$) and wild-type ($N = 4$) mice fasted for 16 h and incubated with $NaHCO_3$ (25 mM), NH_4Cl (10 mM) and ornithine–HCl (5 mM) for 1 h. The amount of urea synthesized was determined by measuring the urea concentration in the media as described in Materials and methods. Values are means ± SEM. $^*P < 0.05$. $^{**}P < 0.01$.

Discussion

In the present study, SIRT5 mRNA levels in liver were found to be increased by fasting. To investigate the function of SIRT5 in liver, we established SIRT5 Tg mice and identified CPS1 as the target protein of SIRT5 by analyses of liver mitochondrial proteins using two-dimensional electrophoresis and MALDI-TOF-MS. We found that CPS1 is deacetylated and that CPS1 activity is significantly increased in the liver of SIRT5 Tg mice. CPS1 is the first and key enzyme of the urea cycle, condensing ammonia with bicarbonate to generate carbamoyl phosphate [15,16]. In hepatocytes from SIRT5 Tg mice, urea synthesis was upregulated compared to that in wild-type mice.

Which residue on CPS1 is deacetylated by SIRT5 is still unclear. The protein that we identified as a target of SIRT5 using two-dimensional electrophoresis and MALDI-TOF-MS was the N-terminal domain of CPS1 (Table. 1), suggesting that the lysine residue of CPS1 deacetylated by SIRT5 is contained in this domain. As Kim et al. reported that CPS1 has nine lysine acetylation sites [26], at least Lys55, Lys119, and/or Lys287 among these lysine residues located in the N-terminal domain might be deacetylated by SIRT5.

During fasting, circulating amino acids, especially alanine, are derived by lysis of muscle proteins, and the amino acids are catalyzed in liver by α-ketoglutarate aminotransferase to generate pyruvate and glutamate. Pyruvate is used in gluconeogenesis to maintain plasma glucose levels, and glutamate is catalyzed by glutamate dehydrogenase to form α-ketoglutarate and ammonia. Ammonia is extremely toxic; the urea cycle converts ammonia to non-toxic urea, which is readily excreted from kidney. It also has been reported that CPS1 activity is increased by fasting or calorie restriction in rodent liver [27,28]. Thus, SIRT5 protein may be involved in detoxification of ammonia during fasting through deacetylation and activation of CPS1.

Recently, Nakagawa et al. reported that CPS1 activity is downregulated in liver of SIRT5 KO mice, which exhibit hyperammonemia by fasting [14]. We show here that CPS1 activity in liver is upregulated in SIRT5 Tg mice during fasting and that urea synthesis is upregulated in SIRT5 Tg hepatocytes, complementing their data.

Suggesting the mechanism of CPS1 activation during fasting, SIRT5 mRNA expression levels in liver were increased by fasting, but protein expression levels were not altered under the same condition in wild-type mice (Supplemental Fig. 1). Nakagawa et al. reported that SIRT5 protein expression levels were not altered, but that NAD levels were elevated by fasting in wild-type mice [14], suggesting that CPS1 is not activated by an increase in SIRT5 protein levels but by activation of SIRT5 through elevation of NAD.

SIRT5 protein is highly expressed in organs other than liver, including kidney, skeletal muscle, and heart (Supplemental Fig. 1), where their functions are yet unknown. Further investigation of the pathophysiological role of SIRT5 is required.

Acknowledgments

This study was supported by Scientific Research Grants from the Ministry of Education, Culture, Sports, Science, and Technology of Japan, from the Ministry of Health, Labor, Welfare, Japan, and by the Kyoto University Global COE Program "Center for Frontier Medicine".

Appendix A. Supplementary data

Supplementary data associated with this article can be found, in the online version, at doi:10.1016/j.bbrc.2010.01.081.

Reference

[1] S. Imai, C.M. Armstrong, M. Kaeberlein, et al., Transcriptional silencing and longevity protein SIR2 is an NAD-dependent histone deacetylase, Nature 403 (2000) 795–800.
[2] M. Kaeberlein, M. McVey, L. Guarente, The SIR2/3/4 complex and SIR2 alone promote longevity in saccharomyces cerevisiae by two different mechanisms, Genes Dev. 13 (1999) 2570–2580.
[3] H.A. Tissenbaum, L. Guarente, Increased dosage of a *sir-2* gene extends lifespan in *Caenorhabditis elegans*, Nature 410 (2001) 227–230.
[4] B. Rogina, S.L. Helfand, SIR2 mediates longevity in the fly through a pathway related to calorie restriction, Proc. Natl. Acad. Sci. USA 101 (2004) 15998–16003.
[5] R.A. Frye, Phylogenetic classification of prokaryotic and eukaryotic SIR2-like proteins, Biochem. Biophys. Res. Commun. 273 (2000) 793–798.
[6] J.T. Rodgers, C. Lerin, W. Haas, S.P. Gygi, et al., Nutrient control of glucose homeostasis through a complex of PGC-1α and SIRT1, Nature 434 (2005) 113–118.
[7] D. Frescas, L. Valent, D. Accili, Nuclear trapping of the forkhead transcription factor FOXO1 via SIRT-dependent deacetylation promotes expression of glucogenetic genes, J. Biol. Chem. 280 (2005) 20589–20595.
[8] Y. Nakamura, M. Ogura, D. Tanaka, et al., Localization of mouse mitochondrial SIRT proteins: shift of SIRT3 to nucleus by co-expression with SIRT5, Biochem. Biophys. Res. Commun. 366 (1) (2008) 174–179.
[9] W.C. Hallows, S. Lee, J.M. Denu, Sirtuins deacetylate and activate mammalian acetyl-CoA synthetases, Proc. Natl. Acad. Sci. USA 103 (2006) 10230–10235.
[10] B. Schwer, J. Bunkenborg, R.O. Verdin, et al., Reversible lysine acetylation controls the activity of the mitochondrial enzyme acetyl-CoA synthetase 2, Proc. Natl Acad. Sci. USA 103 (2005) 10224–10229.
[11] C. Schlicker, M. Gertz, P. Papatheodorou, et al., Substrates and regulation mechanisms for the human mitochondrial sirtuins SIRT3 and SIRT5, J. Mol. Biol. 382 (2008) 790–801.
[12] M.C. Haigis, R. Mostoslavsky, K.M. Haigis, et al., SIRT4 inhibits glutamate dehydrogenase and opposes the effects of calorie restriction in pancreatic beta cells, Cell 126 (2006) 941–954.